DIRECT NUMERICAL SIMULATIONS OF TURBULENT FLOWS GENERATED BY REGULAR AND FRACTAL GRIDS USING AN IMMERSED BOUNDARY METHOD

Sylvain Laizet
Turbulence, Mixing and Flow Control Group, Department of Aeronautics
and Institute for Mathematical Sciences
Imperial College London, London, SW7 2BY, United Kingdom
s.laizet@imperial.ac.uk

J. C. Vassilicos
Turbulence, Mixing and Flow Control Group, Department of Aeronautics
and Institute for Mathematical Sciences
Imperial College London, London, SW7 2BY, United Kingdom
j.c.vassilicos@imperial.ac.uk

ABSTRACT

Two turbulent flows, one generated by a regular grid and the other by a fractal square grid are studied by means of Direct Numerical Simulations (DNS). An innovative approach which combines high order compact schemes, Immersed Boundary Method and an efficient domain decomposition method is used in this study. Turbulent statistics such as Reynolds stresses are investigated with the objective to analyse the two different regions (production and decay regions) downstream from the grid, as already observed in the experimental results of Hurst & Vassilicos (2007). The main goal of this numerical study is to identify the physical mechanisms implicated in the generation of turbulent flows, especially when generated at different scales, but also to compare the different levels of turbulence intensity generated by each grid.

INTRODUCTION

Homogeneous isotropic turbulence has been widely studied experimentally in wind or water tunnels and numerically using tri-periodic boxes with spectral methods. Recently, Hurst & Vassilicos (2007) and Seoud & Vassilicos (2007) used different multiscale grids to generate turbulence in a wind tunnel and have shown that complex multiscale boundary/initial conditions can drastically influence the behaviour of a turbulent flow, especially when a fractal square grid (see figure 1, right) is placed at the entry of a wind tunnel test section. Theses experiments have shown that fractal grids can generate unusually high turbulent intensities compared with regular grids. Moreover, they have also shown that the multiscale nature of a fractal grid can deeply modify the turbulent characteristics of the flow. For example, by playing with the shape and the aspect of a fractal grid, it is possible to tune it as a very efficient inline mixer (high turbulent intensities with small pressure drop, see Coffey *et al.*, 2007).

Although the wind tunnel measurements have provided invaluable time-resolved information on the unique properties of multiscale-generated turbulent flows, to better understand the underlying physics of this new kind of turbulent flows, it is necessary to investigate their full spatial structure. Chester *et al.* (2007) performed renormalized numerical simulation (RNS) on a high-Reynolds number flow over a tree-like fractal to model the drag of the unresolved branches of the fractal tree. However, they did not investigate any turbulent intensities in their simulations. Very recently, Nagata *et al.* (2009) performed DNS of turbulent flows generated by three different fractal grids but with a relatively small Reynolds number. They have been able to recover some of the experimental results of Hurst & Vassilicos (2007), such as the higher turbulent intensities that fractal square grids generate by comparison to regular grids. Impressive advances in parallel platform architectures have allowed Laizet *et al.* (2008) to successfully develop an innovative numerical approach for DNS of multiscale-generated turbulent flows which combines the IBM for the modelling of the grids with high order schemes and a 1-D domain decomposition method. They have also successfully performed DNS of turbulence generated by a fractal cross grid at different spatial resolutions in order to validate their numerical strategy (see Laizet & Vassilicos, 2009).

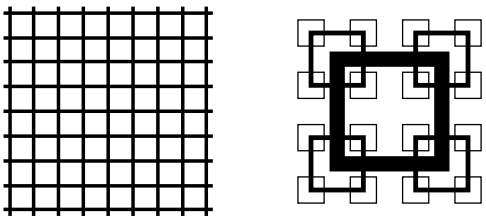

Figure 1: *Scaled diagrams of the fractal square grid (left) and the regular grid (right) used in this numerical study. Note that they have the same blockage ratio.*

In this study, we use DNS to compare turbulent flows generated by regular and fractal square grids in order to investigate the turbulent characteristics of each flow and discover the origins of the non-usual properties of a turbulent flow generated by a fractal square grid previously observed in the experimental data of Hurst & Vassilicos (2007).

The organisation of this paper is as follows. In the following section, we presents the DNS methodology, a brief description of the grids and the numerical parameters of each simulation. Some suggestive flow visualisations are presented and discussed in section after. Then, in order to better understand the underlying properties of each flow, some statistical results are presented in the penultimate section, following by a conclusion in the last section.

FLOW PARAMETERS AND NUMERICAL MODELLING

Numerical methods

To solve the incompressible Navier-Stokes equations, we use a numerical code (called **Incompact3d**) based on sixth-order compact schemes for spatial discretization and second order Adams-Bashforth scheme for time advancement. To treat the incompressibility condition, a fractional step method requires to solve a Poisson equation. The main originality of **Incompact3d** is that this equation is fully solved in spectral space via the use of relevant 3D Fast Fourier Transforms which allow different sets of boundary conditions in each spatial direction: free-slip, periodic, inflow/outflow or Dirichlet boundary conditions on the velocity field. With the help of the concept of modified wave number (Lele, 1992), the divergence free condition is ensured up to machine accuracy.

The modelling of the grids is performed by an Immersed Boundary Method (IBM). Following the procedure proposed by Parnaudeau *et al*. (2003), the present IBM is a direct forcing approach that ensures the no-slip boundary condition at the wall of the grid. Combined with a sixth-order compact filtering of the convective terms, this specific IBM leads to a reduction of wiggles in the neighbourhood of the grid while allowing better quantitative predictions at marginal resolution. A priori, the combination of a high order scheme with the IBM can be problematic because of the discontinuity in velocity derivatives locally imposed by the artificial forcing term. However, even though the formal order of the solution is reduced as a result, the code has been demonstrated to be far more accurate with a 6th order scheme than with a 2nd order scheme both in statistics and instantaneous field realisations (see Parnaudeau *et al*. (2003, 2008) for more details). Furthermore, the Cartesian grid does conform with the geometries of the fractal and regular grids of figure 1 because they consist of right angles and they are placed normal to the mean flow. Note finally that the pressure mesh is staggered from the velocity one to avoid spurious pressure oscillations introduced by the IBM.

More details about the present code and its validation, especially the original treatment of the pressure in spectral space, can be found in Laizet & Lamballais (2008) and Laizet *et al*. (2008).

The highly vectorised version of the code (parallelised with MPI implementation) is used mainly because of the multiscale nature of the fractal square grid. The code's 1D domain decomposition strategy offers two major advantages: the accuracy of the order of our sixth-order schemes has been maintained, and scalability is excellent because, even though our compact schemes are implicit in space, there is no data communication (overlapping) at the boundaries of each subdomain. Furthermore, this domain decomposition is fully compatible with the parallel FFT library named "FFTW" (http://fftw.org). More details about the present parallel method can be found in Sandham & Howard (2004) and in Laizet *et al*. (2008).

Description of the grids

For this numerical study, two different grids are considered: a regular grid which consists of equally distributed equal size bars (see figure 1, left) and a fractal square grid which consists of different sized squares placed in a fractal-like pattern (see figure 1, right). This fractal grid is completely characterised by

- its number of fractal iterations, here $N = 3$
- its bar lengths $L_j = R_L^j L_0$ and thicknesses $t_j = R_t^j t_0$ (in the plane of the grid, normal to the mean flow) at iteration j, $j = 0, ..., N-1$. Here, $R_L = 1/2$, $R_t = 0.584$, $L_0 = 0.5L_y$, where L_y and L_z (with $L_y = L_z$) are the numerical domain's lateral sections of the computational domain (see figure 2).
- its number B^j of patterns at iteration j, here $B = 4$.

By definition, $L_0 = L_{max}$, $L_{N-1} = L_{min}$, $t_0 = t_{max}$ and $t_{N-1} = t_{min}$.

The blockage ratio σ is the same for both grids, $\sigma \approx 32\%$. It is also of interest to define the thickness ratio of each grid: $t_r = t_{max}/t_{min} = 8.5$ for the fractal square grid and $t_r = 1$ for the regular one. Numerically, we set $t_{min} = 1$ in both grids. Unlike the regular grid, the fractal square grid considered here does not have a well-defined mesh size. Hurst & Vassilicos (2007) introduced an effective mesh size for multiscale grids, $M_{eff} = \frac{4T^2}{P}\sqrt{1-\sigma}$ where P is the grid's perimeter length in the $(y-z)$ plane. Note that the fractality of the grid influences M_{eff} via the perimeter P which can be extremely long in spite of being constrained to fit within the area T^2. For the two grids considered here, $M_{eff} = (40/3)t_{min}$. For the fractal square grid, $t_{max} = 0.96M_{eff}$. Note finally that the thickness of the bars in the streamwise direction is $0.19M_{eff}$ for both grids.

The simulations are be performed with the same Reynolds number $Re_{M_{eff}} = 4000$ (based on the effective mesh size M_{eff} of the grids and the streamwise upstream velocity U_∞), blockage ratio and effective mesh size. For the Reynolds number considered here ($Re_{M_{eff}} = 4000$) about 765 million mesh nodes are needed.

Numerical parameters

The numerical parameters of each simulation can be found in Table 1. It is important to notice that the parameters for both simulations are the same the only difference being the shape of the grid. Based on a preliminary study by Laizet & Vassilicos (2009), the streamwise position of the grid ($5t_{min}$ from the inflow boundary of the computational domain) has been carefully chosen to avoid any spurious interactions between the modelling of the grid and the inflow boundary condition (see figure 2 for a schematic view of the flow configuration for the fractal square grid).

Domain ($\times M_{eff}$)	Mesh nodes
$34.56 \times 8.64 \times 8.64$	$2305 \times 576 \times 576$

$Re_{M_{eff}}$	Δt
4000	$5.625\ 10^{-4} M_{eff}/U_\infty$

Table 1: Numerical parameters of both simulations. Note that $L_y = L_z = 8.64M_{eff}$ and $L_x = 4L_y = 34.64M_{eff}$.

Due to the multiscale nature of the fractal square grid, the number of mesh nodes is of crucial importance because all the scales need to be accurately represented. A preliminary study (Laizet & Vassilicos, 2009) has shown that five mesh nodes is enough to discretize the smallest thickness of the fractal square grid for the Reynolds number considered here. This study has also established that the collection time needed in the simulations for good low order statistics is 15 M_{eff}/U_∞. Statistics are obtained by using the

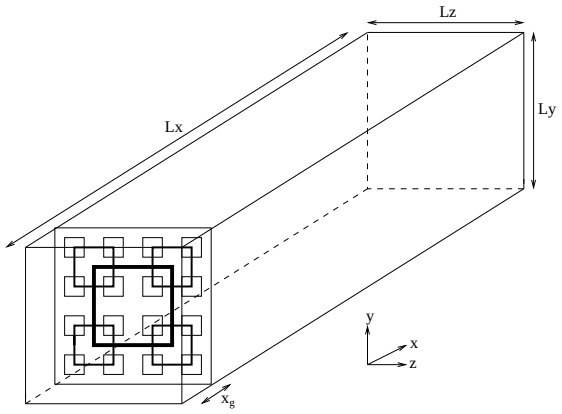

Figure 2: Schematic view of the flow configuration for the fractal square grid.

symmetries of the flow and by averaging over time at given spatial locations. This way, we obtain mean flow and turbulence profiles as functions of streamwise distance x/M_{eff} or lateral coordinate y/M_{eff}.

INSTANTANEOUS FLOW VISUALISATIONS

Instantaneous streamwise velocity visualisations of a turbulent flow generated by the regular grid are given in figures 3 and 4. All the same-size wakes generated by the regular grid interact and mix together very close to the grid, giving rise to a low intensity homogeneous isotropic turbulence within about $20M_{eff}$ from the grid. The fractal square grid generates a more complex turbulent flow due to the multiscale nature of the grid. An illustration of this flow is presented in figures 5 and 6 again in terms of instantaneous streamwise velocity visualisations. A non-homogeneous turbulent field is obtained close to the grid with clear presence of wakes of three different sizes, corresponding to the three fractal iterations of the grid. As already mentioned by Laizet & Vassilicos (2008), these visualisations suggest sequential interactions between wakes from small-scale ones all the way up to larger scale ones. These interactions could be responsible for the prolonged production region observed in the experimental results of Hurst & Vassilicos (2007).

Although the flow generated by the regular grid becomes homogeneous very close to the grid, it is important to note that the fractal square grid can generate much higher turbulence intensities compared with the regular grid even far downstream where the turbulence becomes homogeneous. This is clearly related to the imprint of the fractal grid which remains important far from the grid and strongly influences the turbulent flow. For the regular grid, the imprint disappears relatively quickly whereas the square pattern of the fractal square grid can still be observed at $x = 30M_{eff}$. Note finally that the experimental results of Hurst & Vassilicos (2007) and Seoud & Vassilicos (2007) indicate that homogeneity is reached beyond $x = 60M_{eff}$ with fractal square grids.

STATISTICAL RESULTS

Figure 7 shows the streamwise profiles along the centreline of turbulent Reynolds number $Re_{\lambda_x} = u'\lambda_x/\nu$ based on the Taylor microscale $\lambda_x = u'^2/ < (\partial u/\partial x)^2 >$ and the

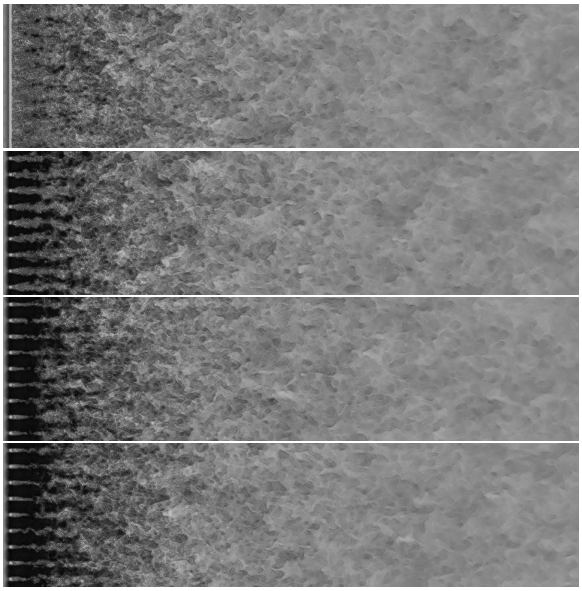

Figure 3: *Instantaneous streamwise velocity of the flow behind the regular grid in the* $(x - z)$ *plane, for* $y =$ 0, 2.16, 1.08 *and* $0.54M_{eff}$ *(Top to bottom). The black color corresponds to* 1.5 *and the white one to* -1.5.

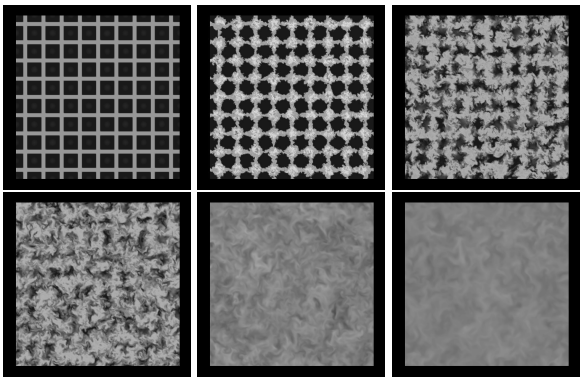

Figure 4: *Instantaneous streamwise velocity of the flow behind the regular grid in the* $(y - z)$ *plane, for* $x =$ 0, 1.2, 3, 4.5, 15 *and* $27M_{eff}$. *The black color corresponds to* 1.5 *and the white one to* -1.5.

r.m.s. u' of the streamwise fluctuating velocity. The fractal square grid generates a Reynolds number Re_{λ_x} more than three times bigger than the classical grid despite the same $Re_{M_{eff}}$, in good agreement with the experimental results of Hurst & Vassilicos (2007). Also, Re_{λ_x} is roughly constant for the classical grid whereas it is decreasing slowly for the fractal square grid, in qualitative agreement with the experimental results of Hurst & Vassilicos (2007) and Seoud & Vassilicos (2007)

In figure 8, we observe two different behaviours for the streamwise evolution of the mean velocity. As expected with the regular grid, U/U_∞ is found to have a wake-like behaviour close to the grid with a small recirculation bubble due to the two crossed bars on the centreline of the grid. After $x \approx 8M_{eff}$, U/U_∞ remains constant with a value very close to 1. For the fractal square grid however, we observe a different streamwise evolution of the mean velocity on the centreline. U/U_∞ is found to peak close to the grid at a

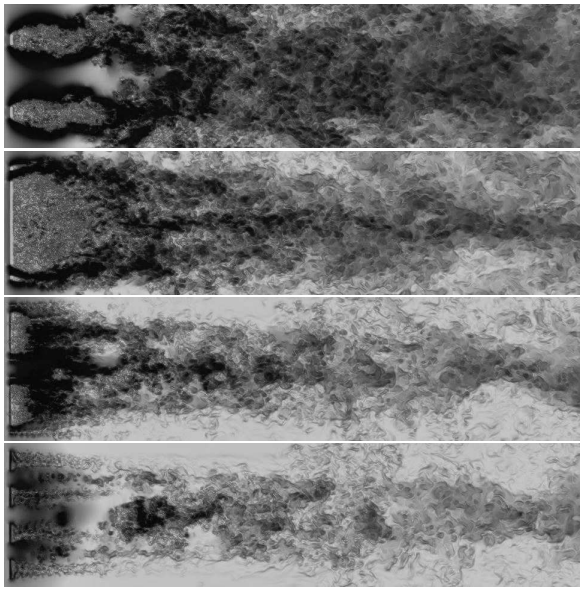

Figure 5: *Instantaneous streamwise velocity of the flow behind the fractal square grid in the* $(x-z)$ *plane, for* $y = 0,\ 2.16,\ 1.08$ *and* $0.54M_{eff}$ *(Top to bottom). The black color corresponds to* 1.5 *and the white one to* -1.5.

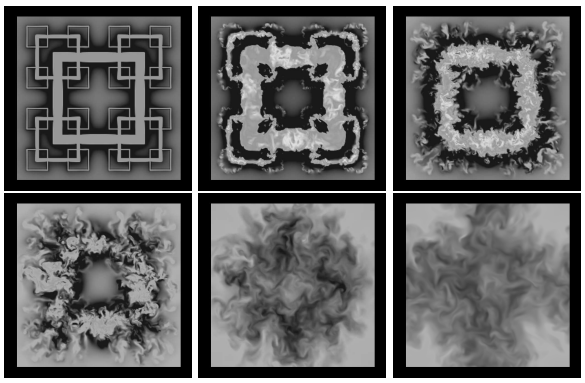

Figure 6: *Instantaneous streamwise velocity of the flow behind the fractal square grid in the* $(y-z)$ *plane, for* $x = 0,\ 1.2,\ 3,\ 4.5,\ 15$ *and* $27M_{eff}$. *The black color corresponds to* 1.5 *and the white one to* -1.5.

value of 1.48, then decays to 1 and remains constant after $x \approx 16M_{eff}$ with a value close to 1.27.

In figure 9 we plot for both grids the development of the turbulent intensities u'/U_∞, v'/U_∞ and w'/U_∞ on the centreline as the turbulence is convected downstream. For the regular grid, the three turbulent intensities have the same behaviour with a strong gradual decrease starting from $x \approx 1M_{eff}$. For the fractal square grid, these turbulent intensities build up until they reach a point $x_{peak} \approx 9.4M_{eff}$, where they peak and then decay beyond that point. Even if the number of fractal iterations is smaller than the experiments, this fundamental result is in good agreement with the experiment of Hurst & Vassilicos (2007) and Seoud & Vassilicos (2007) who also had two regions downstream the grids (production and decay regions) and found that these regions are dependent on the set of parameters defining the fractal square grid. Furthermore, we have performed animations of the streamwise velocity visualizations using more than 500

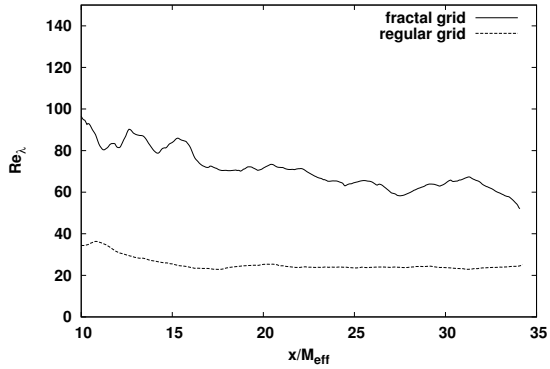

Figure 7: Streamwise profiles of turbulent Reynolds number based on the Taylor microscale on the centreline of both grids.

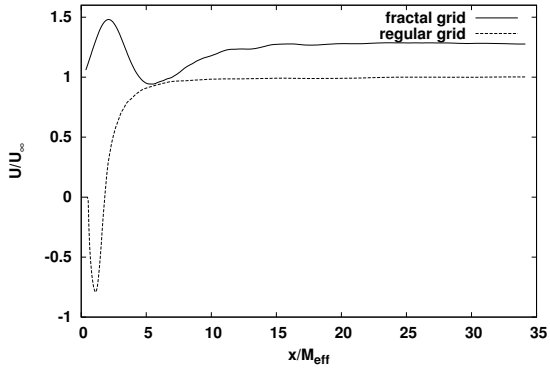

Figure 8: Streamwise profiles of the mean velocity on the centreline of both grids.

velocity fields saved with a period of 2.42 $10^{-2}M_{eff}/U_\infty$. For the fractal square grid, the observation of the animations suggests that the streamwise location of x_{peak} is oscillating between $8.6M_{eff}$ and $10.2M_{eff}$ (the movie is avalaible at http://media.efluids.com/galleries/all?medium=534). It seems that these oscillations are directly linked to the frequency of the big wakes generated by the biggest square of the grid.

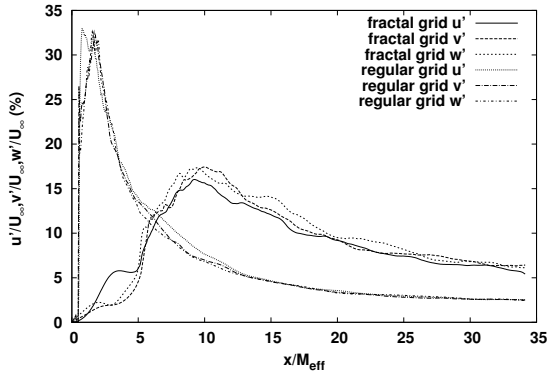

Figure 9: Streamwise profiles of turbulent intensities on the centreline of both grids.

Even if very close to the grid the turbulent intensities are much higher behind the regular grid, it should be noticed

that these turbulent intensities are more than at least twice bigger behind the fractal square grid after $x \approx 10M_{eff}$. Indeed, at the end of the computational domain, we have $u'/U_\infty \approx 6\%$ for the fractal square grid and only $\approx 2.5\%$ for the regular grid. The fractal square grid for the same blockage ratio and same Reynolds number $Re_{M_{eff}}$ is able to generate far downstream much more turbulence than the regular grid.

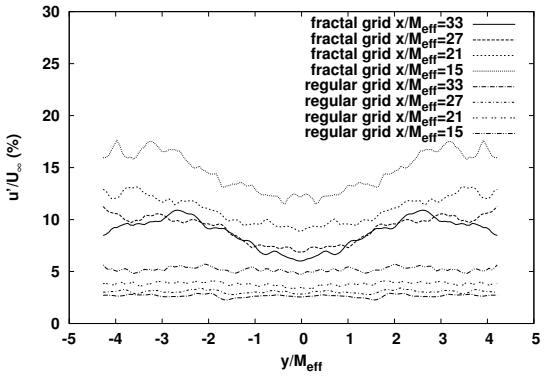

Figure 10: Lateral profiles of the turbulent intensities $u^{'}/U_{infty}$ at $z/M_{eff} = 0$ for $x = 15, 21, 27$ and $33M_{eff}$.

Figure 10 shows that the turbulent intensities are approximately homogeneous across the lateral directions for the regular grid where $x \geq 15M_{eff}$ whereas they are not for the fractal square grid up until $x \approx 33M_{eff}$. Indeed, we observe a small increase of the turbulent intensities near the lateral boundaries of the computational domain, probably resulting from the biggest square of the grid. These two peaks seem to move toward the centreline of the grid: at $x = 15M_{eff}$, the peaks are at $y = \pm 3.4M_{eff}$ and at $x = 33M_{eff}$, they are at $y = \pm 2.8M_{eff}$. It should be noted that, as already shown on the centreline, the fractal square grid generates much higher turbulent intensities than the regular grid, for the same Reynolds number $Re_{M_{eff}}$. For example, at $x = 33M_{eff}$, $u'/U_\infty \approx 8.5\%$ for the fractal square grid near the lateral boundaries and only $\approx 2.5\%$ for the regular grid (3.4 times bigger).

In figure 11, we plot the lateral and diagonal profiles for each grid of the mean velocity at 4 different streamwise locations. The mean velocity profile for the fractal square grid is not uniform in the lateral and diagonal directions as it has a jet-like inhomogeneity whereas the respective profile for the regular grid is clearly homogeneous. The results are in good agreement with the experimental results of Hurst & Vassilicos (2007) (see figure 35*a* of their paper) despite a number of fractal iterations reduced from 4 to 3. They suggest that the inhomogeneities are jet-like because fractal square grids are characterized by a clear empty strip in the region near the centreline in the z direction. Note finally that we have checked that $\frac{1}{L_y L_z}\int_{-L_y/2}^{L_y/2}\int_{-L_z/2}^{L_z/2} \mathbf{u} dydz = U_\infty$ for many planes normal to the streamwise direction.

Some of these initial observations can be investigated a bit further in terms of frequency power spectra of the streamwise velocity (figure 12). These power spectra, obtained on the centreline at four different streamwise locations, are calculated using the periodogram technique (see Press *et al.* (1992) for more details about this technique). Eleven sequences are used here, corresponding to a global time duration equal to $28.35M_{eff}/U_\infty$ overlapped at 50%, with the use of a Hanning window. Close to the grid ($x = 4.5M_{eff}$),

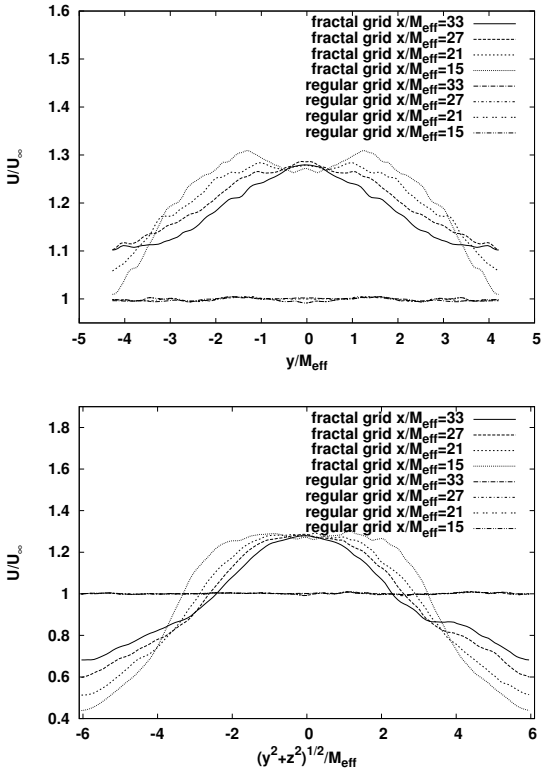

Figure 11: Lateral (top) and diagonal (bottom) profiles of the mean velocity U/U_∞ for $x = 15, 21, 27$ and $33M_{eff}$. The lateral profiles are at $z = 0$ and the diagonal ones are along the $y = z$ line.

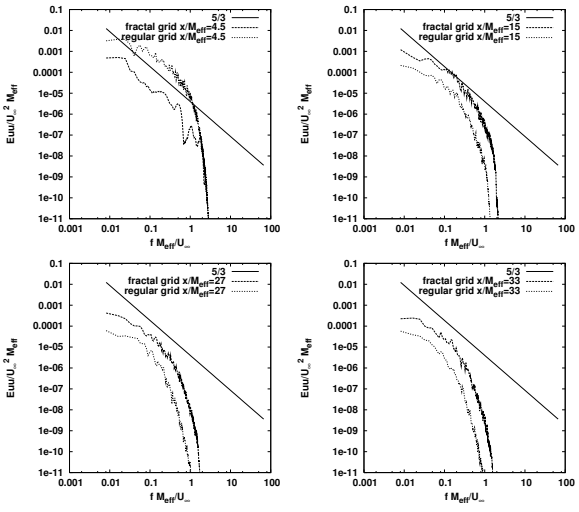

Figure 12: *Power spectra of the streamwise velocity on the centreline of the grids for* $x = 4.5,\ 15,\ 27$ *and* $33M_{eff}$.

the flow is clearly not fully turbulent for the fractal square grid and not fully homogeneous for the regular grid, yet a $-5/3$ scaling region exists in both cases. For the three other streamwise location, and in agreement with the previous observations, the power spectra for the fractal square grid take much larger values than those for the regular grid.

CONCLUSION

Two spatially evolving turbulent flows generated by a regular and a fractal square grid have been investigated by means of DNS. One of the main results is that the fractal square grid is able to generate much higher turbulent intensities than a regular grid for the same Reynolds number $Re_{M_{eff}}$ and the same blockage ratio. For the fractal square grid, we have been able to recover the two different regions already observed in the experiments of Hurst & Vassilicos (2007): a production region where the flow is non-homogeneous and where the turbulence peaks followed by a decay region.

Further DNS will be required to investigate in more detail the spatial evolution of the turbulent flow generated by a fractal square grid. First, it could be interesting to experiment with the ability of fractal grids to independently control pressure drop and turbulence intensity. It is possible to tune them as very efficient mixers if pressure drop is made low by lowering blockage ratio whilst making turbulence intensities high by increasing the thickness ratio t_r between successive fractal iterations (See Coffey *et al*, 2007 and Hurst & Vassilicos, 2007). Alternatively, it might be possible to tune them as silent airbrakes if the pressure drop is made high and turbulence intensity low. Coffey *et al* (2007) have already shown in their water tunnel investigations that fractal square grids can be designed as stirring elements for inline static mixers and that they compare favourably with commercially available state-of-the-art stirring elements.

Another future direction of investigation concerns the behaviour of the turbulence in the decay region. In their experimental measurements, Hurst & Vassilicos (2007) and Seoud & Vassilicos (2007) have shown that, beyond the peak position, the turbulence decays freely but in a way that is qualitatively, as well as quantitatively, different from any turbulence decay previously observed in experiments and simulations: the turbulence decays exponentially (which means slowly to start with and eventually fast) with both macro and micro flow length-scales approximately constant along the decay region. The turbulence in these experiments is homogeneous for $x > x_{peak}$, which is not the case in the current simulation. However, the number of fractal iterations is 3 here whereas it is equal to 4 or 5 in these experiments. Hence, this number seems to play a role in the distance from the grid where the turbulence becomes homogeneous. This will be investigated in the future. Finally, a large range of t_r will need to be studied with different numbers of fractal iterations and larger Reynolds numbers $Re_{M_{eff}}$ so as to be closer to the experimental measurements of Hurst & Vassilicos (2007) and Seoud & Vassilicos (2007).

ACKNOWLEDGMENTS

We acknowledge the EPSRC grant EP/F051468 and the UK Turbulence consortium for the CPU time made available to us on HECToR without which this study would not have been possible. The authors are grateful to Roderick Johnstone and Vincent Hurtevent for help with the parallel version of **Incompact3d**. We also thank Eric Lamballais for very useful discussions and acknowledge support from EPSRC Research grant EP/E00847X.

REFERENCES

Coffey C.J., Hunt G.R., Seoud R.E. & Vassilicos J.C., 2007 "Mixing effectiveness of fractal grids for inline static mixers", *Proof of Concept report for the attention of Imperial Innovations.* http://www3.imperial.ac.uk/tmfc/papers/poc

Chester S., Meneveau C. & Parlange M. B., 2007 "Modeling turbulent flow over fractal trees with renormalized numerical simulation", *J. Comp. Phys.* **225** doi:10.1016/j.jcp.2006.12.009

Hurst D. & Vassilicos J.C., 2007 "Scaling and decay of fractal-generated turbulence", *Phys. Fluids* **19**,035103. http://link.aip.org/link/?PHFLE6/19/035103/1

Laizet S., Lamballais E. & Vassilicos J.C., 2008 "A numerical strategy to combine high-order schemes, complex geometry and massively parallel computing for the DNS of fractal generated turbulence", (*Submitted to Computers & fluids*) http://www3.imperial.ac.uk/tmfc/papers/preprints

Laizet S. & Lamballais E., 2008 "High-order compact schemes for incompressible flows: a simple and efficient method with the quasi-spectral accuracy", (*In revision J. Comp. Phys.*)

Laizet S. & Vassilicos J.C., 2009 "Multiscale generation of turbulence", *J. of Multiscale Modelling*, **1** 177-196 http://www3.imperial.ac.uk/tmfc/papers/2009

Laizet S. & Vassilicos J.C., 2008 "Direct Numerical Simulation of fractal-generated turbulence", *Proc. DLES-7, Trieste, September.*

Lele S.K., 1992 "Compact finite difference schemes with spectral-like resolution",*J. Comp. Phys.*, **103** 16-42 doi:10.1016/0021-9991(92)90324-R

Nagata, K., Suzuki, H., Sakai, Y., Hayase & Kubo, T., 2009 "Direct Numerical Simulation of Turbulence Characteristics Generated by Fractal Grids", *In press in Inter. Review of PHYSICS.*

Parnaudeau P., Carlier J., Heitz D. & E. Lamballais, 2008 "Experimental and numerical studies of the flow over a circular cylinder at Reynolds number 3 900", *Phys. Fluids* **20** ,085101.

Parnaudeau P., Lamballais E. & Silvestrini J.H., 2003 "Combination of the immersed boundary method with compact schemes for DNS of flows in complex geometry", *Proc. DLES-5, Munich.*

Press W.H., Teukolsky S.A., Vetterling W.T. and Flannery B.P., 1992 "Numerical Recipes", *Cambridge University Press, Cambridge.*

Sandham N. D. and R. J. A. Howard R. J. A., 1998 "DNS of turbulence using massively parallel computers", *Computational Fluid Dynamic, D. R. Emerson and A. Ecer and J. Periaux and N. Satofuka and P. Fox*, 23–32.

Seoud R.E. & Vassilicos J.C., 2007 "Dissipation and decay of fractal-generated turbulence", *Phys. Fluids* **19**, 105108. http://link.aip.org/link/?PHFLE6/19/105108/1